Particle entanglement spectra for quantum Hall states on lattices

Antoine Sterdyniak

Laboratoire Pierre Aigrain, Ecole Normale Supérieure, 45 rue Lhomond, F-75005 Paris, France

Nicolas Regnault

Department of Physics, Princeton University, Princeton, New Jersey 08544, USA and
Laboratoire Pierre Aigrain, Ecole Normale Supérieure, 45 rue Lhomond, F-75005 Paris, France

Gunnar Möller

TCM Group, Cavendish Laboratory, J. J. Thomson Avenue, Cambridge CB3 0HE, United Kingdom

We use particle entanglement spectra to characterize bosonic quantum Hall states on lattices, motivated by recent studies of bosonic atoms on optical lattices. Unlike for the related problem of fractional Chern insulators, very good trial wave functions are known for fractional quantum Hall states on lattices. We focus on the entanglement spectra for the Laughlin state at $\nu = 1/2$ for the non-Abelian Moore-Read state at $\nu = 1$. We undertake a comparative study of these trial states to the corresponding ground states of repulsive two-body or three-body contact interactions on the lattice. The magnitude of the entanglement gap is studied as a function of the interaction strength on the lattice, giving insight into the nature of Landau-level mixing. In addition, we compare the performance of the entanglement gap and overlaps with trial wave functions as possible indicators for the topological order in the system. We discuss how the entanglement spectra allow to detect competing phases such as a Bose-Einstein condensate.

I. INTRODUCTION

Optical lattices present unique opportunities to simulate the physics of charged particles in strong magnetic fields.[1] While early proposals for artificial gauge fields relied on rotation to mimic the action of Lorentz forces by the Coriolis forces acting in the rotating frame,[2,3] optical lattices provide a robust experimental setting where the effect of fields can be simulated by imprinting complex phases on tunneling elements between neighboring sites.[4–6] The most elegant schemes for generating synthetic gauge fields in atomic gases rely on the use of Berry phases resulting from a set of internal states subject to a spatially varying optical dressing.[7–9] In particular, these schemes enable the generation of high densities of flux per plaquette on the underlying lattice, giving access to a regime of strong correlation where exotic topologically ordered phases can appear, including fractional quantum Hall liquids such as the Laughlin state[6,10] and more exotic Hall liquids which rely on the presence of the lattice.[11–13]

A related class of lattice models relies on spin-orbit coupling to generate complex hopping terms in single-particle tight-binding Hamiltonians. If the resulting single-particle bands are flat and have a nonzero Chern number, these systems can support states resembling fractional quantum Hall (FQH) liquids that are known as fractional Chern insulators (FCI).[14–17] Fractional Chern insulators have been most convincingly shown to exhibit the same type of topological order as FQH states by analyzing their particle entanglement spectra.[18]

The entanglement spectra (ES) were initially introduced by Li and Haldane[19] in the context of the FQHE, stimulating an extensive range of studies.[18,20–34] They have also been studied and applied to several other systems including spin systems,[35–45] as well as topological insulators[46–48] Bose-

Hubbard models,[49] or complex paired superfluids.[50] The ES corresponds to the spectrum of the reduced density matrix of the system ground state when one cuts the system into two parts. The system partition can be performed in different manners such as a real-space, momentum, or particle-space partition. Each cut can unveil different aspects of the state that is probed. In the case of the FQHE, the ES are related to the bulk or edge excitations. As these features characterize the given phase, the ES acts as a fingerprint of the system that only requires knowledge of the ground-state wave function.

For the above reasons, the ES were found to be particularly well suited as a tool to characterize FCI states as they only require knowledge of the ground-state wave function which can be obtained numerically for small model systems.[18] Hence, it was possible to establish a detailed correspondence between the entanglement spectra of FCI with those of fractional quantum Hall states.[51] In particular, it has recently been shown[52] that the ES is able to distinguish between a Laughlin-like state and a charge-density wave state (CDW). However, an important difference is that for fractional quantum Hall states, very accurate analytic many-body trial wave functions capturing the essence of these strongly correlated quantum liquids are known,[53–57] so a very detailed understanding of the topological order and the fundamental excitations in FQH systems has been achieved. We note that mappings of FQH wave functions onto topological flat bands[58–62] have recently led to some encouraging results, including considerable overlaps with FCI eigenstates[59,60] and the demonstration of an analytic continuation between these systems.[60,62]

In this paper, we focus on quantum Hall states on lattices with a homogeneous density of gauge flux, as this gives us access to a lattice-based system where quantum Hall states can be understood both in terms of entanglement spectra and many-body trial wave functions. As opposed to FCIs, quantum

Hall states on lattices admit a continuum limit which is known to be exactly the usual FQHE. We deploy exact numerical diagonalization on a square lattice with periodic boundary conditions as the main tool for our investigation. Our study provides an independent identification of the incompressible phases on the lattice as fractional quantum Hall states by analyzing the counting of quasiparticle states in the particle entanglement spectrum. To obtain the expected state counting, we establish the correspondence between the momentum sectors of a lattice-based system with periodic boundary conditions and the corresponding continuum problem on the torus. We find that for small enough particle density n per lattice site, the counting of the continuum problem is accurately reproduced. In particular, this allows us to mount evidence in favor of the non-Abelian Moore-Read state as the ground state of bosons with repulsive three-body interactions at filling factor $\nu = 1$ on the lattice. Finally, we study how the entanglement gap, defined as the distance between the eigenvalues of the entanglement spectrum related to the universal property of the bulk excitations and the nonuniversal states at higher entanglement energy, relates to the magnitude of the overlap with the respective trial wave functions describing the target phase. This establishes the entanglement gap as a good proxy for the overlap, and hence for the stability of topological order.

The structure of this paper is as follows. In Sec. II, we introduce the model Hamiltonian for bosons on lattices in the presence of magnetic fields and with periodic boundary conditions. Section III is devoted to a discussion of the corresponding continuum FQHE problem on the torus, where we introduce the many-body wave functions of the target phases which we explore in this paper, namely the Laughlin state (Sec. III A) and the Moore-Read state (Sec. III B). We then review the definition and characteristics of entanglement spectra in Sec. IV, and present a detailed analysis of the particle entanglement spectra of our two target phases in Sec. V. In the case of the Laughlin state, we describe how certain features of the ES can be used as a probe to detect a competing Bose-Einstein condensed phase. Finally, our results are summarized in Sec. VI.

II. MODEL

We study the physics of interacting bosons on a two-dimensional square lattice in a homogeneous magnetic field applied in the direction perpendicular to the lattice. This problem is described by the Bose-Hubbard model with minimal coupling to a gauge field by Peierls' substitution. We further assume the presence of on-site two-body interactions of strength U and three-body interactions of strength V, yielding the many-body Hamiltonian

$$\mathcal{H} = -t \sum_{\langle \mathbf{r}, \mathbf{r}' \rangle} (e^{i A_{\mathbf{r}\mathbf{r}'}} \hat{a}_{\mathbf{r}}^{\dagger} \hat{a}_{\mathbf{r}'} + \text{H.c.})$$

$$+ U \sum_{\mathbf{r}} \hat{a}_{\mathbf{r}}^{\dagger} \hat{a}_{\mathbf{r}}^{\dagger} \hat{a}_{\mathbf{r}} \hat{a}_{\mathbf{r}} + V \sum_{\mathbf{r}} \hat{a}_{\mathbf{r}}^{\dagger} \hat{a}_{\mathbf{r}}^{\dagger} a_{\mathbf{r}}^{\dagger} \hat{a}_{\mathbf{r}} \hat{a}_{\mathbf{r}} \hat{a}_{\mathbf{r}}. \tag{1}$$

Here, $\langle \mathbf{r}, \mathbf{r}' \rangle$ denotes neighboring lattice sites $\mathbf{r} = (x, y)$, $\hat{a}_{\mathbf{r}}^{(\dagger)}$ are bosonic annihilation (creation) operators, and $A_{\mathbf{r}\mathbf{r}'} = \int_{\mathbf{r}}^{\mathbf{r}'} \mathbf{A} \cdot d\mathbf{l}$ are Aharonov-Bohm phases deriving from the coupling to the underlying vector potential $\mathbf{A}$. We adopt units such that the

lattice spacing is 1, and positions (x, y) can be indicated as integers.

Experimentally, bosonic Hubbard models can be engineered in optical lattices systems,[63] where gauge potentials can be simulated by a range of different setups.[4–9] Two-body interactions can be conveniently introduced by Feshbach resonances,[64,65] and there are proposals for three-body interactions based on strong three-particle losses.[66,67] Given this pace of progress in simulating Hubbard models, Hamiltonians of the form (1) may be realizable within the near future.

For our numerical exact diagonalization calculations, we express the Hamiltonian (1) for an ensemble of N bosons on a square lattice with $N_s = L_x L_y$ sites in the presence of N_ϕ flux quanta and with periodic boundary conditions in both the x and y directions. This setup corresponds to a field of flux density $n_\phi = N_\phi / N_s$, which we choose to describe in the Landau gauge

$$\mathbf{A} = 2\pi n_\phi x \mathbf{e}_y, \tag{2}$$

such that momentum in the y direction is a conserved quantity. Due to the concurrence of a periodic lattice potential, periodic boundary conditions, and the presence of a magnetic field, this translational symmetry is reduced[68] to the possible momenta of $k_y = 2m\pi / K_y^{\max}$, $m = 0, \ldots, K_y^{\max} - 1$ with the maximal momentum index given by the greatest common denominator

$$K_y^{\max} = \gcd(N_\phi, L_y). \tag{3}$$

This can be simply explained by applying Blochs theorem to magnetic unit cells enclosing an integer number of flux quanta. Due to the reduced symmetry, the orbitals are labeled by a sublattice index s for the y position inside the magnetic unit cell in addition to the momentum k_y. Both interaction terms in Eq. (1) conserve this Landau momentum, so the Hamiltonian is block diagonal and we construct the eigenstates in the Fock space given by $|\alpha\rangle = \prod_\zeta (\hat{a}_\zeta^{\dagger})^{n_\zeta(\alpha)} |0\rangle$, where $\zeta = (x, k_y, s)$ denotes the set of single-particle quantum numbers.

We should stress that this set of states does not imply a projection to the lowest Landau level. Instead, it includes all of the bands of the fractal single-particle spectrum known as the Hofstadter butterfly,[69] such that Landau-level mixing is part of the model. The equivalent Landau-level filling (i.e., the particle density with respect to the number of states in the lowest band) is given by $\nu = N / N_\phi$.

III. FQH ON THE TORUS

We now briefly describe some properties of the FQHE in the torus geometry. We consider a torus spanned by $\mathbf{L}_1 = L_x' \mathbf{e}_x$ and $\mathbf{L}_2 = L_y' \mathbf{e}_y$, where $\mathbf{e}_x$ and $\mathbf{e}_y$ are two perpendicular unit vectors. Given a setting where the torus is pierced by N_ϕ flux quanta, we have $L_x' L_y' = 2\pi l_B^2 N_\phi$, where l_B is the magnetic length. The Hamiltonian is given by

$$H = \frac{1}{2m} \sum_i^N \Pi_i^2 + U \sum_{i<j} \tilde{\delta}(\mathbf{r}_i - \mathbf{r}_j)$$

$$+ V \sum_{i<j<k} \tilde{\delta}(\mathbf{r}_i - \mathbf{r}_j) \tilde{\delta}(\mathbf{r}_j - \mathbf{r}_k), \tag{4}$$

where $\mathbf{\Pi}_i = -i\hbar \nabla_i - e\mathbf{A}(\mathbf{r}_i)$ is the canonical momentum of particle j in the presence of a magnetic field. Since we use

periodic boundary conditions, the delta function is defined as $\tilde{\delta}(\mathbf{r}) = \sum_{n,m} \delta(\mathbf{r} + n\mathbf{L}_1 + m\mathbf{L}_2)$.

In the Landau gauge ($\mathbf{A} = 2\pi n_\phi x \mathbf{e}_y$), the one-particle orbital in the lowest Landau level with momentum index $j = 0, \ldots, N_\phi - 1$ is given by

$$\phi_j(x,y) = \frac{1}{(\sqrt{\pi} L_y' l_B)^{1/2}} \exp\left[-\frac{x^2}{2l_B^2}\right]$$
$$\times \vartheta \begin{bmatrix} \frac{j}{N_\phi} \\ 0 \end{bmatrix} \left(\frac{N_\phi}{L_y'}(y - ix) \middle| i\frac{L_x'}{L_y'}\right), \qquad (5)$$

where $\vartheta[{}^a_b](z|\tau) = \sum_n e^{i\pi\tau(n+a)^2 + 2i\pi(n+a)(z+b)}$ are the generalized Jacobi theta functions. This model is the continuous version of Eq. (1).

As for the lattice, the momentum in the y direction is a conserved quantity and the N-body Hamiltonian is block diagonal with respect to the total momentum $\mathcal{K}_y^T = \sum_i j_i \bmod N_\phi$. Note that in the case of the lattice, the total momentum $\mathcal{K}_y$ is defined modulo $K_y^{\max}$.

A. Laughlin state

In the lowest Landau level, when only two-body interactions are present [i.e., $V = 0$ in Eq. (4)], the Laughlin state is the densest zero-energy ground state.[53] A hallmark of this phase is its two-fold ground-state degeneracy. For a finite size system with $N_\phi = 2N$ the two ground states can be found at momenta of $\mathcal{K}_y^T = 0, N$. They are given by

$$\Psi(z_1, \ldots, z_N) = f_{\text{rel}}(z_1, \ldots, z_N) F_{\text{c.m.}}(Z) e^{-\frac{1}{2}\sum_i x_i^2/l_B^2}, \qquad (6)$$

where $F_{\text{c.m.}}$ is a center-of-mass wave function that depends only on the center-of-mass coordinate $Z = \sum_i z_i$, while f_{rel} is the wave function describing the relative motion. On a rectangular torus of size ($L_x' \times L_y'$), we have

$$f_{\text{rel}} = \prod_{i<j} \vartheta \begin{bmatrix} \frac{1}{2} \\ \frac{1}{2} \end{bmatrix} \left(\frac{z_i - z_j}{L_y'} \middle| i\frac{L_x'}{L_y'}\right)^2. \qquad (7)$$

Due to the symmetry under translations of the center of mass, the center-of-mass wave function at $\nu = 1/2$ is two-fold degenerate[70] and is given by

$$F_{\text{c.m.}}(Z) = \vartheta \begin{bmatrix} \frac{l}{2} + \frac{N_\phi - 2}{4} \\ \frac{2 - N_\phi}{2} \end{bmatrix} \left(\frac{2Z}{L_y'} \middle| 2i\frac{L_x'}{L_y'}\right), \qquad (8)$$

where $l = 0, 1$ indexes the two degenerate wave functions.

B. Moore-Read state

In the lowest Landau level, the Moore-Read state[55] is the densest zero-energy ground state of the hardcore three-body interactions, given by Eq. (4) with $U = 0$. It embodies the physics of a chiral p-wave superconductor of composite fermions,[71,72] which can be cast in the real-space form of a BCS paired state in terms of the pair wave function $1/(z_i - z_j)$. An equivalent expression can be found for the torus, where the ground state is three-fold degenerate. On a rectangular torus, these ground states can be found at k_y momenta $\mathcal{K}_y^T = \{0, 0, \frac{N}{2}\}$. For our purposes, it is most useful to obtain the Moore-Read trial wave functions from the Laughlin state by

using the Cappelli formula,[73] which relates the Moore-Read state of N particles to two independent layers of Laughlin $\nu = 1/2$ states with half the number of particles. Using the notations for a sphere or disk

$$\Psi_{\text{Pf}}(z_1, \ldots, z_N)$$
$$= \mathcal{S}\left(\prod_{i<j=2}^{N/2} (z_i - z_j)^2 (z_{\frac{N}{2}+i} - z_{\frac{N}{2}+j})^2\right), \qquad (9)$$

where $\mathcal{S}$ is the symmetrization operator. On the torus, the Laughlin state is two-fold degenerate while the Moore-Read state is three-fold degenerate. Similar to what happens for the quasihole states on the disk or sphere geometry, the symmetrization induces linear dependencies. Here one can write four states:

$$\Psi_{K_y^T}^{\text{Pf}}(z_1, \ldots, z_N) = \mathcal{S}\left(\Psi_{K_{y_1}^T}^{Lg}(z_1, \ldots, z_{N/2})\right.$$
$$\left. \times \Psi_{K_{y_2}^T}^{Lg}(z_{N/2+1}, \ldots, z_N)\right), \qquad (10)$$

with $K_{y_1}^T, K_{y_2}^T$ being equal to one of the degenerate Laughlin states with $K_y^T = 0$ or $K_y^T = N' = \frac{N}{2}$. The total momentum $K_y^T = K_{y_1}^T + K_{y_2}^T \bmod N_\phi$ perfectly matches the one of the Moore-Read (MR) state: Taking $K_{y_1}^T = K_{y_2}^T = 0$ yields a first $K_y^T = 0$ MR state, taking $K_{y_1}^T = K_{y_2}^T = N'$ again yields $K_y^T = 0$, and finally taking $K_{y_1}^T = 0$ and $K_{y_2}^T = N'$ one obtains the remaining MR ground state at $K_y^T = N' = N/2$ state (choosing $K_{y_1}^T = N'$ and $K_{y_2}^T = 0$ is equivalent due to the symmetrization and does not yield an additional state).

IV. PARTICLE ENTANGLEMENT SPECTRA

The entanglement spectrum gives access to many of the spectral properties of the system which are encoded in the ground-state wave function.[19] It is defined from the reduced density matrix of a subsystem resulting from the partition of the system into two (or more) parts A and B. For the particle entanglement spectrum (PES) this partition consists in distributing the particles into two subgroups (A and B) while keeping the geometry unchanged.[74] The reduced density matrix $\rho_A = \text{Tr}_B\rho$, obtained by tracing out the N_B particles in the B partition, yields the entanglement spectrum by diagonalizing and classifying the resulting eigenstates according to the symmetries of the problem. This process is equivalent to a Schmidt decomposition of the original many-body state into orthogonal bases for the partitions

$$|\Psi\rangle = \sum_\varpi \sum_i e^{-\xi_{\varpi,i}/2} |\Psi_{\varpi,i}^A\rangle \otimes |\Psi_{\varpi,i}^B\rangle, \qquad (11)$$

where ϖ stands for quantum numbers designating a sector of the decomposition and i indexes states in each sector, and the eigenvalues $\lambda_{\varpi,i} = e^{-\xi_{\varpi,i}/2}$ of the decomposition are represented on a logarithmic scale. The vectors in Eq. (11) are orthonormal [i.e., $\langle \Psi_{\varpi,i}^A | \Psi_{\varpi',j}^A \rangle = \langle \Psi_{\varpi,i}^B | \Psi_{\varpi',j}^B \rangle = \delta_{i,j}\delta_{\varpi,\varpi'}$]. The entanglement spectrum is given by plotting ξ's over the relevant ϖ.

It has been observed that model states such as the Laughlin or MR states have a characteristic PES:[74] The number of nonzero eigenvalues for ρ_A is identical to the number of

quasihole states for a similar system with the same geometry and N_A particles. This number is usually exponentially lower than the dimension of ρ_A. The same features can often persist for eigenstates of realistic interaction Hamiltonians: for ground-state wave functions with robust topological order, one should observe a clearly defined entanglement gap, separating an ensemble of low-lying entanglement eigenvalues from nonuniversal eigenvalues located at higher entanglement energies. Notice that model wave functions can be thought of as having an infinite entanglement gap.

For the model associated to the Hamiltonian (1), we classify the sectors of the entanglement spectrum by the Landau momentum $k_y = 0, \ldots, K_y^{\max} - 1$ (i.e., $\varpi = k_y$). An equivalent classification can be chosen for the continuum fractional quantum Hall problem on the torus,[70] except that the corresponding Landau momentum $\mathcal{K}_y^T$ can take all N_ϕ distinct values. To compare the entanglement spectra in these two distinct situations, we identify the momentum sectors modulo $K_y^{\max}$. In particular, we will study the counting of the number $\mathcal{N}$ of low-lying entanglement eigenvalues below an entanglement gap. In this case, we expect the following mapping between the values for the torus $\mathcal{N}_T$ and lattice $\mathcal{N}_L$:

$$\mathcal{N}^L(k_y) = \sum_{\mathcal{K}_y^T} \delta_{k_y,(\mathcal{K}_y^T \bmod K_y^{\max})} \mathcal{N}^T(\mathcal{K}_y^T). \quad (12)$$

Note that for degenerate ground-state manifolds, the PES has to be calculated for the incoherent average reduced density matrix ρ_{tot} for the ensemble of ground states $\{|\Psi_\alpha\rangle\}$, given by the sum

$$\rho_{\text{tot}} = \frac{1}{d_{\text{GS}}} \sum_\alpha |\Psi_\alpha\rangle\langle\Psi_\alpha| \quad (13)$$

over the d_{GS} degenerate ground states. As discussed in Ref. 74, this definition yields model state PES for degenerate ground-state manifolds which recover the properties of the nondegenerate case on simply connected surfaces.

V. TARGET PHASES

The presence of incompressible fractional quantum Hall liquids is well established for the Hamiltonian (1). These states include the fractional quantum Hall liquids of the continuum

problem,[6,10] however, the presence of the lattice potential also gives rise to additional incompressible states.[11–13] In this paper, our aim is to establish the use of entanglement spectra for lattice-based systems, so we shall focus on the states with an equivalent in the continuum case and undertake a comparison of their features.

A. Laughlin state

We begin our analysis with the Laughlin state of bosons at $\nu = 1/2$, as the best investigated quantum Hall state on lattices. We use the analytic form of the Laughlin states in the continuum [Eq. (6)] and substitute the discrete lattice coordinates, such that $z = a/\ell_0(m\mathbf{e}_x + in\mathbf{e}_y)$ for lattice site $\mathbf{i} = (m,n)$. By virtue of the folding of momenta (3), the two ground states (8) now occur at $k_y = 0$ and $k_y = N \bmod K_y^{\max}$ (i.e., they may either remain at different k points or are both mapped to zero momentum if $N \bmod K_y^{\max} = 0$). In our simulations, we find that for lattice systems with sufficiently small particle density, the momenta of the numerically obtained ground states are in agreement with this prediction. In particular, there is an extended regime where a two-fold degenerate ground state with a finite gap is found.[10] Hence, we can analyze the particle entanglement spectrum of the ground-state manifold according to the total density matrix (13).

We begin to illustrate the mapping of the entanglement spectrum on the torus to the lattice (12) for a small model system with $N = 6$ particles moving in the field of $N_\phi = 12$ flux quanta. We first consider the PES with $N_A = 3$. Figure 1(a) shows the PES for the Laughlin state on the torus geometry. The PES yields the following counting for the 12 distinct $\mathcal{K}_y^T$-momentum sectors on the torus: (10,9,9,10,9,9,10,9,9,10,9,9). Figure 1(b) displays the PES for the ground state of the model Hamiltonian that gives rise to the Laughlin state, but with an additional small contribution from a longer-range interaction. In that case, the PES exhibits a entanglement gap. The counting below the gap exactly matches the one of the Laughlin state.

We now consider the lattice model. The counting of the Laughlin on the torus is reproduced exactly on a lattice of geometry $L_x = 4$ and $L_y = 12$ for $U/t = 1$ and $V = 0$ [see Fig. 2(a)] as this lattice retains $K_y^{\max} = N_\phi = 12$. Notice that the total number of states above the gap per momentum sector
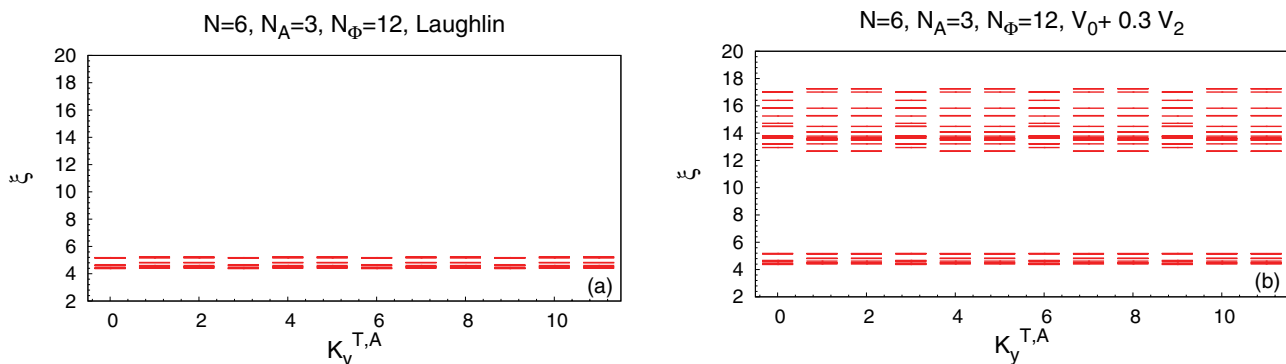

FIG. 1. (Color online) Particle entanglement spectra for $N = 6$ bosons on the torus of unity aspect ratio at filling factor $\nu = N/N_\phi = 1/2$, for a particle partition with $N_A = 3$. Left: Bosons interact through hardcore interaction. Right: Bosons interact through hardcore interaction and an additional longer-range interaction.
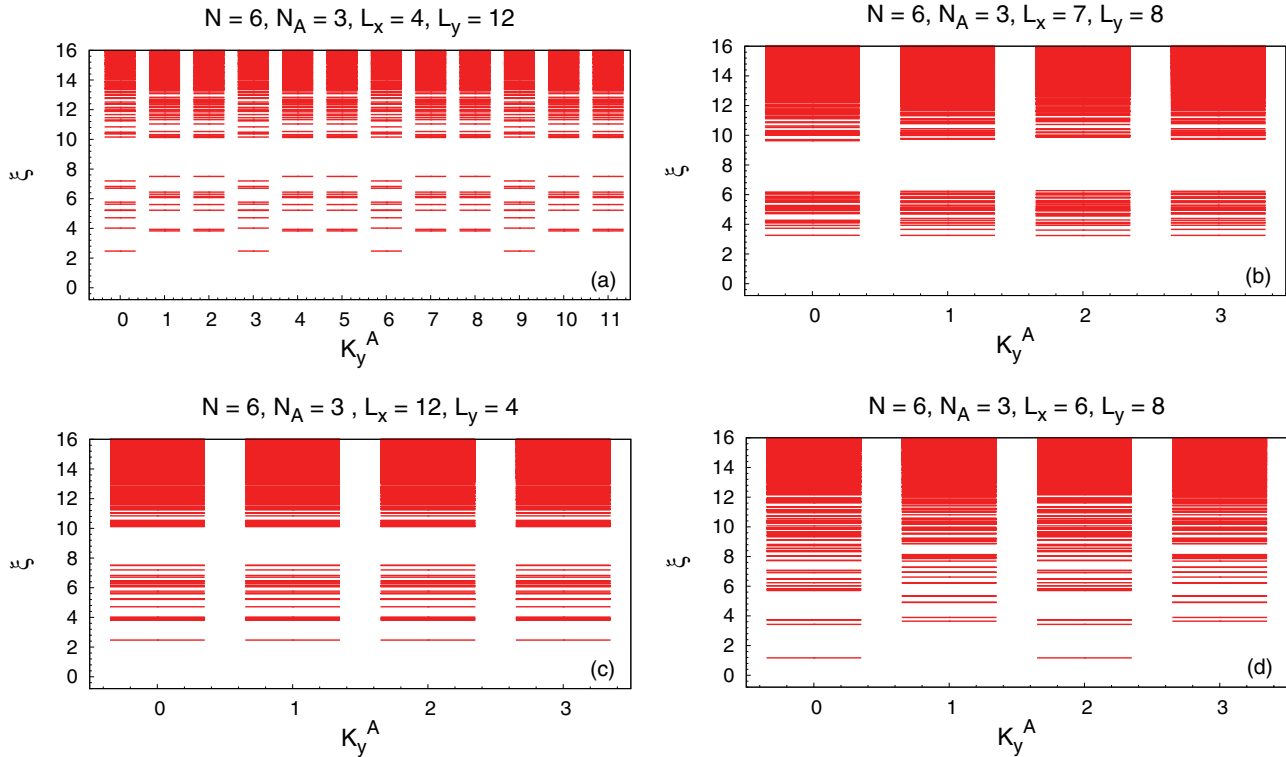
FIG. 2. (Color online) Particle entanglement spectra for $N = 6$ bosons on a lattice at filling factor $\nu = N/N_\phi = 1/2$, for a particle partition with $N_A = 3$ and for different lattice geometries. The spectra are calculated for the two-fold degenerate ground-state manifold of the Hamiltonian (1) with $U/t = 1$ and $V = 0$.

is much higher in the lattice case than in the continuum model shown in Fig. 1(b). This is a consequence of the Hilbert space dimension being set by N and $L_x \times L_y$ in the lattice case, and by N and N_ϕ in the continuum case. So our confirmation of a clear entanglement gap for such a small number of particles in the lattice model is even more remarkable.

For lattices with other aspect ratios, a folding of the momentum axis often occurs, in which case the maximum momentum is reduced. Several examples for such entanglement spectra are shown in Figs. 2(b) through 2(d). For example, in Fig. 2(b), for the geometry with $L_x = 7$, $L_y = 8$, and $K_{\max} = 4$ the use of Eq. (12) predicts the counting (28,28,28,28), which is indeed reproduced. The same result is also obtained for the aspect ratio of 12×4 sites in Fig. 2(c). However, we do not always obtain a PES with a well-defined entanglement gap. For the lattice geometry of $L_x = 6$ and $L_y = 8$, we find that no threshold value ξ_t for the entanglement energy yields a clear-cut definition of $\mathcal{N}_{\xi_t}^L(k_y)$. We could speculate whether this is due to the commensurability of the number of particles with L_x. In such geometries, it has previously been found that CDW states can intervene.[12] However, there is a range of phases which may be competing with fractional quantum Hall liquids in optical flux lattices, which include bosonic condensates with symmetry breaking,[75] or more general supersolid phases.[75,76]

As a first step towards understanding the lattice which does not conform to the picture of an incompressible Laughlin state ($L_x = 6$, $L_y = 8$), we investigate several additional entanglement spectra for this system, analyzing the dependency on the number of particles in the partition A. The results for $N_A = 1$ and $N_A = 2$ are shown in Fig. 3. First, we note

that the entanglement spectrum for $N_A = 1$ carries nontrivial information for the lattice, while the corresponding continuum limit would yield a number of eigenstates which is given by the total Hilbert space dimension (i.e., the number of states in the lowest Landau level). On the lattice, we instead find that a gap opens in the entanglement spectrum above a number of low-lying states which precisely matches the number of eigenstates in the lowest Landau level. Specifically, Fig. 3(a) reveals precisely 12 states below the gap located at about $\xi = 6$. For a Laughlin state, we would expect all 12 of these states to be degenerate. Second, we find that there are two eigenstates which are separated from the other ten by a further entanglement gap located near $\xi = 2$, reproducing the same number and momentum sectors $K_y^A = 0$ and $K_y^A = 2$ of the two low-lying states that we had observed in the PES for $N_A = 3$ in Fig. 2(d). To complete our survey, we also examine the entanglement spectrum for $N_A = 2$ in Fig. 3(b). Again, we find two degenerate low-lying eigenstates with an entanglement gap near $\xi = 2$ and located in the same momentum sectors. This invariance of the number of entanglement eigenvalues with the number of particles in the partition is fundamentally different from the behavior that we expect from topologically ordered phases. By contrast, the ability to absorb further particles without any change of the physical properties (i.e., the number of low-lying excitations) can be seen as an indication of the physics of Bose condensation.

To probe for the presence of a Bose condensate, we use the single-particle density matrix $\rho_{ij}^s = \langle \hat{a}_i^\dagger \hat{a}_j \rangle$, calculated between lattice sites i, j. This matrix is exactly a reduced density matrix for the specific value $N_A = 1$. A state with
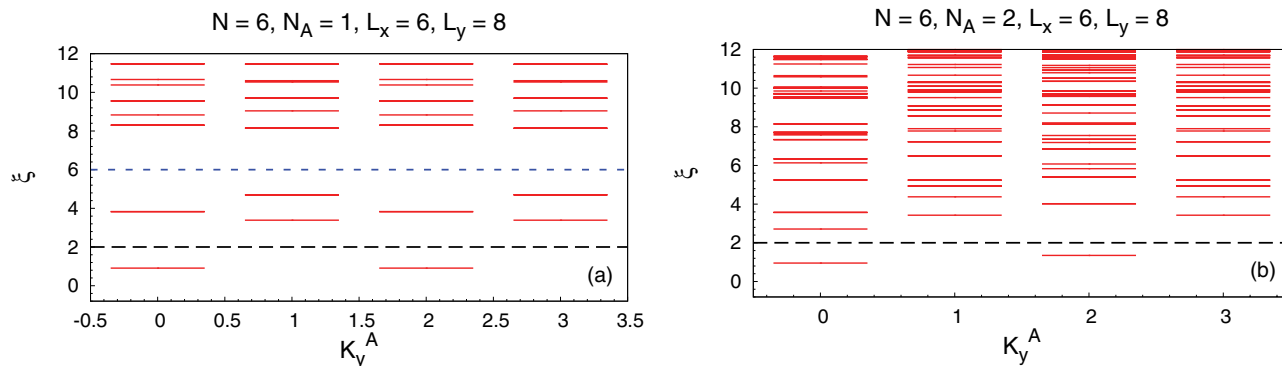
FIG. 3. (Color online) Particle entanglement spectra for $N = 6$ bosons on a lattice of 6×8 sites at filling factor $\nu = N/N_\phi = 1/2$ for particle partitions with (a) $N_A = 1$ and (b) $N_A = 2$ [$N_A = 3$ shown in Fig. 2(d)]. For $N_A = 1$, the upper blue dashed line marks the entanglement gap below which the counting matches the lowest Landau level state counting of 12 states, and the lower black dashed line marks the entanglement gap that isolated the two low-lying eigenstates. For $N_A = 2$, the black dashed line marks the entanglement gap that isolated the two low-lying eigenstates.

a finite condensate fraction is signalled by a single large eigenvalue λ_0 of ρ^s, whose magnitude scales with the system size N. However, we find that the ground-state wave function for our system with $L_x = 6$ and $L_y = 8$ and $N_\phi = 12$ yields a two-fold degenerate pair of largest eigenvalues $\lambda_0 = \lambda_1 \simeq 2.472$. This characteristic is known to be associated to discrete symmetry breaking in the thermodynamic limit.[75] We thus follow the procedure introduced by the authors of Ref. 75 and calculate the density matrix for symmetry-broken states which are obtained in our case by constructing superpositions formed of the two lowest-lying eigenstates $|S\rangle = c_0|\Psi_0\rangle + (1 - |c_0|^2)|\Psi_1\rangle$ that optimize the largest eigenvalue of ρ_{ij}^s. For the symmetry-broken state that results from superposing

two states with different momenta, we find a single large density matrix eigenvalue $\lambda_0(S) = 4.4911$, corresponding to a condensed fraction of 74.8% for the $N = 6$ particle system (the condensate fraction rises to 95% as interactions are reduced to $U = 0.1t$). At the same time, the state breaks translational invariance, forming stripes running around the short cycle of the simulation cell. A similar finite size effect had previously been reported for lattices,[12] as well as for continuum problems of bosons.[77] It is likely that the properties of the particular lattice size which we discuss here are related to its flux density of precisely $n_\phi = 1/4$. At this value of n_ϕ, the single-particle Hofstadter spectrum consists of a single, moderately wide band which naturally supports Bose condensation at low

TABLE I. Properties of the particle entanglement spectra of the ground-state manifold of the Hamiltonian for $U/t = 1$ and $V = 0$ (1) for different model systems of N bosons with $N_\phi = 2N$ flux quanta. We indicate the momenta of the two degenerate ground states k_y(GS) as well as the energy gap Δ and the ground-state energy splitting δ. The counting of the particle entanglement spectrum is shown for the partition with $N_A = \lfloor N/2 \rfloor$ and for different lattice geometries. For both these properties, we indicate the agreement with the predictions for the Laughlin state and the entanglement gap Δ_ξ.

N	L_x	L_y	k_y(GS)	match	Δ	δ	PES: $\{\mathcal{N}_{AL}(k_y)\}$	match	Δ_ξ
4	4	4	0,0	✘					
4	6	4	0,0	✘					
4	8	4	0,0	✓	0.043	5.9e-04	6,4,6,4	✓	3.59
4	14	4	0,0	✓	0.058	1.8e-05	6,4,6,4	✓	7.42
4	6	6	0,0	✓	0.050	0.023	12,8	✓	4.86
4	4	8	0,4	✓	0.043	5.9e-04	3,2,3,2,3,2,3,2	✓	3.59
4	6	8	0,4	✓	0.066	7.1e-04	3,2,3,2,3,2,3,2	✓	8.1
4	7	8	0,4	✓	0.057	2.9e-10	3,2,3,2,3,2,3,2	✓	10.9
4	8	8	0,4	✓	0.052	0	3,2,3,2,3,2,3,2	✓	11.5
4	10	8	0,4	✓	0.040	1.4e-08	3,2,3,2,3,2,3,2	✓	12.9
5	6	8	0,1	✓	0.059	0	20,15	✓	5.5
5	8	8	0,1	✓	0.063	0	20,15	✓	9.2
5	6	10	0,5	✓	0.067	0	4,3,4,3,4,3,4,3,4,3	✓	8.4
6	4	12	0,6	✓	0.054	0	10,9,9,10,9,9,10,9,9,10,9,9	✓	2.63
6	12	4	0,2	✓	0.054	0	28,28,28,28	✓	2.63
6	6	8	0,2	✓	0.0099	0.0029	$\Delta_E = 0$	✘[a]	
6	7	8	0,2	✓	0.043	8e-6	28,28,28,28	✓	3.5

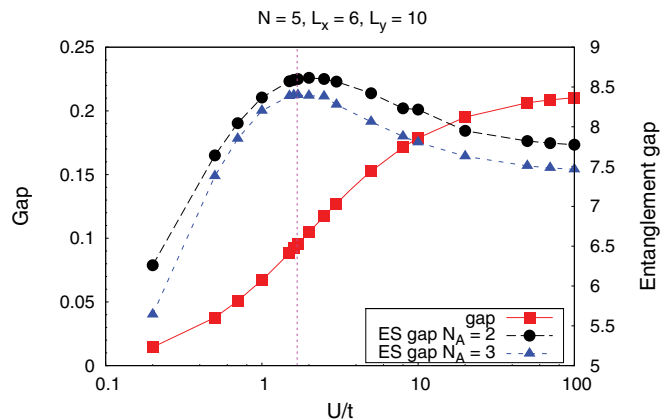[a]See Fig. 3 and main text in Sec. V A for a discussion.

FIG. 4. (Color online) Energy gap Δ and entanglement gap Δ_ξ in the $N_A = 2$ and in the $N_A = 3$ sectors as a function of U for $\nu = 1/2$, $N = 5$, $L_x = 6$, and $L_y = 10$. The vertical purple line is the band gap. Note the different offsets on the scales for Δ and Δ_ξ.

interaction strength. As we do not examine this question in further detail, we can only speculate whether all of the above features survive in the thermodynamic limit, in which case the phase could be considered a supersolid.[75] For the purpose of the current paper, we can conclude that an entanglement spectrum with few low-lying states, whose number remains invariant for different partitions of the system, is indicative of a condensed state. Cases where such eigenvalues occur in different momentum sectors are likely related to condensates with symmetry breaking.

Returning to our main discussion of the properties of the Laughlin state, we present a collection of the properties of the entanglement spectra in Table I, which gives an overview for several lattice geometries that we have studied. To summarize our principal findings from these data, we have established that the counting of excitations encoded in the PES for the Laughlin states on the lattice Hamiltonian at filling factor $\nu = 1/2$ agrees well with the data for the continuum problem in the lowest Landau level for small flux/particle density per plaquette. In particular, the entanglement spectra of this state show a clear entanglement gap Δ_ξ.
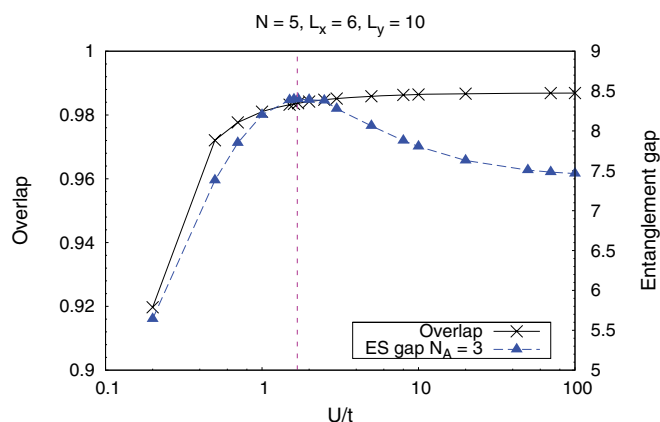

FIG. 6. (Color online) Entanglement gap Δ_ξ as a function of flux density n_ϕ for the Laughlin state with $N = 5$ particles. The vertical dotted line indicates the critical value $n_\phi^c \simeq 0.4$ up to which the ground state exhibits the Chern number of the Laughlin state (Ref. [10]).

Unlike the problem on the torus, where it is customary to consider the projection of the Hamiltonian into the lowest Landau level, the full lattice Hamiltonian (1) includes all Landau (Hofstadter) bands. Hence, we can study the effect of band mixing that occurs as a function of the interaction strength U. The evolution of the entanglement gap Δ_ξ with U is shown in Fig. 4, alongside the energy gap Δ. Unlike the energy gap which always increases with U, the entanglement gap reaches a maximum value for an interaction strength of the order of the band gap and then decreases.

We also computed the total overlaps $\mathcal{O}_{\text{tot}} = \frac{1}{d} \sum_{i,j=1}^{d} |\langle \Psi_{\text{GS},i} | \Psi_{\text{model},j} \rangle|^2$ of the exact ground states with the model state as a function of the interaction strength. The results are shown on Fig. 5. One can notice that the overlaps are very high. Moreover, the overlap is an increasing function of U, as is the energy gap.

It is now well established that the presence of an entanglement gap, in conjunction with the specific state counting in the PES, characterizes the topological order in the system.

FIG. 5. (Color online) Overlap $\mathcal{O}$ and entanglement gap Δ_ξ in the $N_A = 3$ sectors as a function of U for $\nu = 1/2$, $N = 5$, $L_x = 6$, and $L_y = 10$. The vertical purple line is the band gap. Note the different offsets on the scales for $\mathcal{O}$ and Δ_ξ.
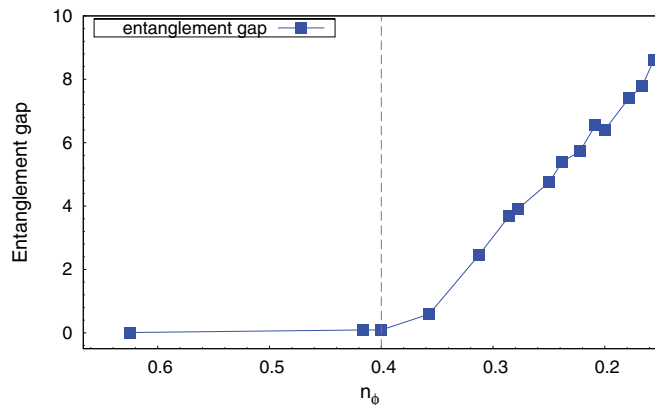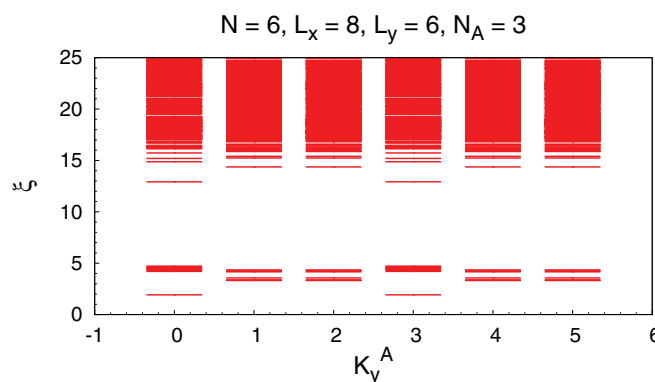

FIG. 7. (Color online) Particle entanglement spectra for $N = 6$ bosons on a lattice at filling factor $\nu = N/N_\phi = 1$, for a particle partition with $N_A = 3$ and for different lattice geometries. The spectra are calculated for the three-fold degenerate ground-state manifold of the Hamiltonian (1) with $U = 0$ and $V/t = 1$. Left: The counting of the states below the gap is (7,6,7,6,6). It matches the one of MR quasiholes states on the torus as $K_y^{\max} = N_\phi$.

TABLE II. Properties of the particle entanglement spectra of the ground-state manifold of the Hamiltonian for $U = 0$ and $V/t = 1$ (1) for different model systems of N bosons with $N_\phi = N$ flux quanta. We indicate the momenta of the three degenerate ground states k_y(GS) as well as the energy gap Δ and the ground-state energy splitting δ. The counting of the particle entanglement spectrum is shown for the partition with $N_A = \lfloor N/2 \rfloor$ and for different lattice geometries. For both these properties, we indicate the agreement with the predictions for the Moore-Read state and the entanglement gap Δ_ξ.

N	L_x	L_y	k_y(GS)	match	Δ	δ	PES: $\{\mathcal{N}_{AL}(k_y)\}$	match	Δ_ξ
4	5	4	0,0,2	✓	0.016	0.005	(3,2,3,2)	✓	7.4
4	9	4	0,0,2	✓	0.015	4.2e-06	(3,2,3,2)	✓	14.2
4	10	4	0,0,2	✓	0.005	3.1e-04	(3,2,3,2)	✓	15.3
4	4	6	0,0,0	✗					
4	6	6	0,0,0	✓	0.011	0.0012	(6,4)	✓	11.8
4	8	6	0,0,0	✓	0.0063	1.7e-05	(6,4)	✓	14.1
4	10	6	0,0,0	✓	0.0036	1.0e-06	(6,4)	✓	16.0
4	4	8	0,0,2	✓	0.01	1.7e-05	(3,2,3,2)	✓	13.0
4	6	8	0,0,2	✓	0.006	1.7e-05	(3,2,3,2)	✓	14.2
4	8	8	0,0,2	✓	0.0042	1.3e-07	(3,2,3,2)	✓	15.2
6	6	4	0,0,1	✓	0.044	0.036	(19,19)		0.39
6	8	4	0,0,1	✓	0.017	0.0085	(19,19)		0.38
6	6	6	0,0,3	✓	0.015	1.3e-04	(7,6,6,7,6,6)	✓	8.2
6	8	6	0,0,3	✓	9.4e-3	3e-5	(7,6,6,7,6,6)	✓	8.2

We are therefore interested to test how this measure compares to other signatures of topological order, such as the presence of a nonzero Chern number for the ground-state manifold. A prior study of the Laughlin state on lattices had shown that the combined two-fold ground-state manifold has a Chern number of 1, or 1/2 per state, up to a critical flux density of $n_\phi^c \simeq 0.4$ (Ref. 10). We now study how the entanglement gap varies as the flux density changes, by calculating entanglement spectra for systems of constant N on lattices of different geometries. The results, shown in Fig. 6, show a full agreement with Ref. 10: For large U, we find that the entanglement gap also closes at $n_\phi^c \simeq 0.4$. However, while the Chern number jumps instantaneously between integers, the entanglement gap can capture how the topological protection of the Laughlin state is gradually weakened and finally collapses.

B. Moore-Read state

We next considered the Moore-Read (MR) state at $\nu = 1$. In the continuum, as explained in Sec. III B, the three MR states can be obtained from the Laughlin state by symmetrization. On the lattice, the same scheme applies except that the momentums are now defined modulo K_y^{max}, and we use the Laughlin states on the lattice as defined in Eqs. (6) through (8) as the starting point.

Our numerical work on the lattice is based on the exact diagonalization of the Hamiltonian (1), using three-body contact interactions which are analogous to the continuum case [i.e., choosing $U = 0$ and $V/t = 1$ in Eq. (1)]. Given these parameters, we generally found that the ground state is approximately three-fold degenerate and the sectors in which the three ground states appear are given by the expected momenta, subject to the folding rule (12). For geometries where this rule is satisfied, we compute the particle entanglement spectrum of the ground states' total density matrix. As in the Laughlin case, the particle entanglement spectrum is gapped and the number of states below the gap is given by the one

predicted from the folding rule and the torus counting [see Fig. 7(a)]. The results for the different systems we studied are gathered in Table II.

These results show that it is theoretically possible to obtain the Moore-Read phase on the lattice using three-body contact interactions. Even though three-body interactions can be realized for cold atoms using more elaborate experimental settings,[66,67] the most relevant interaction for bosons on a lattice is the two-body hardcore interaction. Thus, we wonder if the Moore-Read state can also be stabilized with this type of interaction. In the continuum limit and in the lowest Landau-level (LL) approximation, they are several numerical evidences that such a phase can be stabilized.[78–81] Given the presence of LL mixing mixing in our model, we also establish to which extent this mixing affects the stability of the Moore-Read state. To answer these questions, we diagonalize the Hamiltonian (1) with $V = 0$ at $\nu = 1$. For small interaction strength U, the energy spectrum exhibits the correct ground-state degeneracy
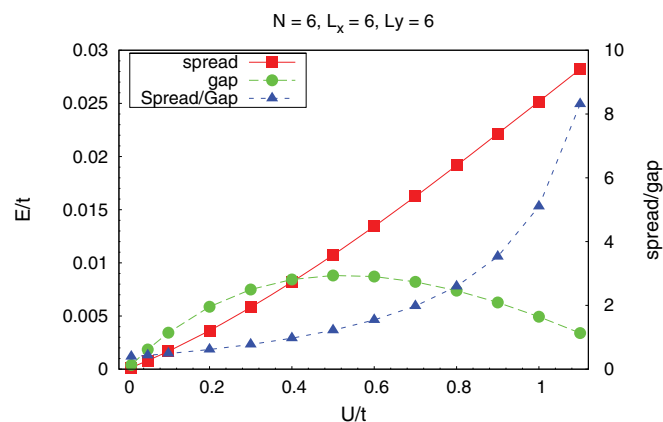

FIG. 8. (Color online) Energy gap $\Delta = E_3 - E_2$ and ground-state energy splitting $\delta = E_2 - E_0$ as a function of U for $\nu = 1$, $N = 6$, $L_x = 6$, and $L_y = 6$, as well as their dimensionless ratio.
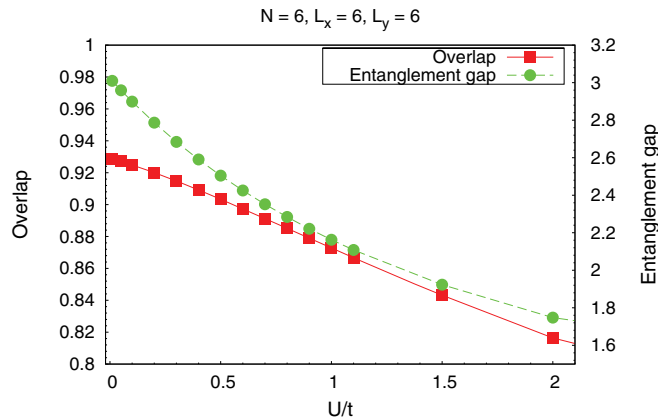
FIG. 9. (Color online) Overlap $\mathcal{O}$ and entanglement gap Δ_ξ in the $N_A = 3$ sectors as a function of U for $\nu = 1$, $N = 6$, $L_x = 6$, and $L_y = 6$. Note the different offsets on the axes for the overlap $\mathcal{O}$ and entanglement gap Δ_ξ.

and sectors. In addition, the entanglement spectra exhibit the correct state counting, albeit with a smaller entanglement gap than in the case of three-body interactions. A closer look at the spectrum reveals, as displayed in Fig. 8, that the energy gap and the ground-state energy splitting are of the same order: While a fully realized MR phase should have a very small spread to gap ratio, this is clearly not the case here.

We find that the gap closes for $U_c \simeq 1.25t$, while the spread between the ground states grows monotonically with U. Hence, the spread to gap ratio is a rapidly increasing function of U indicating how sensitive the topological degeneracy is to the strength of two-body interactions. At the flux density $n_\phi = 1/6$ shown in Fig. 8, the lowest Landau level is still very narrow,[13,69] so we interpret this strong suppression of the gap as resulting from Landau-level mixing. Furthermore, the single-particle gap between the lowest Landau level (LLL) and second LL is about $\Delta_{sp} \simeq 1.68t$ at $n_\phi = 1/6$, which is of the same order as the energy scale of interactions nU_c at the point U_c where the gap closes. We can conclude, at least for small systems, that the Landau-level mixing resulting from large two-body contact interactions tends to destroy the MR phase.

Finally, we have computed the entanglement gap of the total matrix density, taking the two lowest-energy state in the $K_y = 0$ sector and the lowest in the $K_y = N/2$ sector even when they were not the three lowest-energy eigenstates. For reference, we also evaluate the overlap of these states with the

model MR states, as discussed above. The results, shown in Fig. 9, are consistent with the previous conclusions: The phase obtained at small U is most likely the MR phase, with large overlaps at small U, but the phase is destroyed by increasing the interaction strength.

VI. CONCLUSION

In this paper we have analyzed the bosonic fractional quantum Hall states on lattices through the particle entanglement spectrum. These systems provide a well-controlled environment away from the pure model states, which allows a better understanding of the properties of particle entanglement spectra (PES) in quantum Hall systems. We have focused on the filling factors $\nu = \frac{1}{2}$ and $\nu = 1$ where the Laughlin state and the Moore-Read state should, respectively, emerge. In both cases, the PES was able to discriminate the nature of the state. This result is even more remarkable given that the size of the Hilbert space, set by the number of particles and lattice sites (rather than flux quanta), is exponentially larger than in the continuum limit. Interestingly, the PES was able to give insight about a competing Bose-Einstein condensate phase, which we have associated with low-lying entanglement eigenstates whose number is invariant under the number of particles in the partition. We have also shown that the entanglement gap collapse in the PES predicts a critical density of flux n_ϕ^c below which the Laughlin's physics emerges; our value of n_ϕ^c is in agreement with a previous study based on Chern numbers. We have used the PES to confirm the realization of a Moore-Read state at $\nu = 1$ in the presence of on-site two-body contact interactions only. Furthermore, we have given evidence of how Landau-level mixing arising from these two-body contact interactions tends to destroy the bosonic MR state as its magnitude is increased.

[1] J. Dalibard, F. Gerbier, G. Juzeliūnas, and P. Öhberg, Rev. Mod. Phys. **83**, 1523 (2011).

[2] N. R. Cooper and N. K. Wilkin, Phys. Rev. B **60**, R16279 (1999).

[3] N. R. Cooper, Adv. Phys. **57**, 539 (2008).

[4] D. Jaksch and P. Zoller, New J. Phys. **5**, 56 (2003).

[5] E. J. Mueller, Phys. Rev. A **70**, 041603 (2004).

[6] A. S. Sørensen, E. Demler, and M. D. Lukin, Phys. Rev. Lett. **94**, 086803 (2005).

[7] Y. Lin, R. Compton, K. Jimenez-Garcia, J. Porto, and I. B. Spielman, Nature (London) **462**, 628 (2009).

[8] N. R. Cooper, Phys. Rev. Lett. **106**, 175301 (2011).

[9] N. R. Cooper and J. Dalibard, Europhys. Lett. **95**, 66004 (2011).

[10] M. Hafezi, A. S. Sørensen, E. Demler, and M. D. Lukin, Phys. Rev. A **76**, 023613 (2007).

[11] R. N. Palmer and D. Jaksch, Phys. Rev. Lett. **96**, 180407 (2006).

[12] G. Möller and N. R. Cooper, Phys. Rev. Lett. **103**, 105303 (2009).

[13] L. Hormozi, G. Möller, and S. H. Simon, Phys. Rev. Lett. **108**, 256809 (2012).

[14] T. Neupert, L. Santos, C. Chamon, and C. Mudry, Phys. Rev. Lett. **106**, 236804 (2011).

[15] K. Sun, Z.-C. Gu, H. Katsura, and S. DasSarma, Phys. Rev. Lett. **106**, 236803 (2011).

[16] E. Tang, J.-W. Mei, and X.-G. Wen, Phys. Rev. Lett. **106**, 236802 (2011).

[17] D. N. Sheng, Z.-C. Gu, K. Sun, and L. Sheng, Nat Commun **2**, 389 (2011).

[18] N. Regnault and B. A. Bernevig, Phys. Rev. X **1**, 021014 (2011).

[19] H. Li and F. D. M. Haldane, Phys. Rev. Lett. **101**, 010504 (2008).

[20] N. Regnault, B. A. Bernevig, and F. D. M. Haldane, Phys. Rev. Lett. **103**, 016801 (2009).

[21] O. S. Zozulya, M. Haque, and N. Regnault, Phys. Rev. B **79**, 045409 (2009).

[22] A. M. Läuchli, E. J. Bergholtz, J. Suorsa, and M. Haque, Phys. Rev. Lett. **104**, 156404 (2010).

[23] R. Thomale, A. Sterdyniak, N. Regnault, and B. A. Bernevig, Phys. Rev. Lett. **104**, 180502 (2010).

[24] R. Thomale, B. Estienne, N. Regnault, and B. A. Bernevig, Phys. Rev. B **84**, 045127 (2011).

[25] M. Hermanns, A. Chandran, N. Regnault, and B. A. Bernevig, Phys. Rev. B **84**, 121309 (2011).

[26] A. Chandran, M. Hermanns, N. Regnault, and B. A. Bernevig, Phys. Rev. B **84**, 205136 (2011).

[27] E. Ardonne and N. Regnault, Phys. Rev. B **84**, 205134 (2011).

[28] A. Sterdyniak, B. A. Bernevig, N. Regnault, and F. D. M. Haldane, New J. Phys. **13**, 105001 (2011).

[29] Z. Liu, E. J. Bergholtz, H. Fan, and A. M. Läuchli, Phys. Rev. B **85**, 045119 (2012).

[30] A. Sterdyniak, A. Chandran, N. Regnault, B. A. Bernevig, and P. Bonderson, Phys. Rev. B **85**, 125308 (2012).

[31] J. Dubail, N. Read, and E. H. Rezayi, Phys. Rev. B **85**, 115321 (2012).

[32] I. D. Rodriguez, S. H. Simon, and J. K. Slingerland, Phys. Rev. Lett. **108**, 256806 (2012).

[33] J. Schliemann, Phys. Rev. B **83**, 115322 (2011).

[34] V. Alba, M. Haque, and A. M. Läuchli, Phys. Rev. Lett. **108**, 227201 (2012).

[35] P. Calabrese and A. Lefevre, Phys. Rev. A **78**, 032329 (2008).

[36] F. Pollmann and J. E. Moore, New J. Phys. **12**, 025006 (2010).

[37] F. Pollmann, A. M. Turner, E. Berg, and M. Oshikawa, Phys. Rev. B **81**, 064439 (2010).

[38] R. Thomale, D. P. Arovas, and B. A. Bernevig, Phys. Rev. Lett. **105**, 116805 (2010).

[39] A. M. Läuchli and J. Schliemann, Phys. Rev. B **85**, 054403 (2012).

[40] H. Yao and X.-L. Qi, Phys. Rev. Lett. **105**, 080501 (2010).

[41] J. I. Cirac, D. Poilblanc, N. Schuch, and F. Verstraete, Phys. Rev. B **83**, 245134 (2011).

[42] I. Peschel and M.-C. Chung, Europhys. Lett. **96**, 50006 (2011).

[43] C.-Y. Huang and F.-L. Lin, Phys. Rev. B **84**, 125110 (2011).

[44] J. Lou, S. Tanaka, H. Katsura, and N. Kawashima, Phys. Rev. B **84**, 245128 (2011).

[45] J. Schliemann and A. M. Läuchli, arXiv:1205.0109.

[46] L. Fidkowski, Phys. Rev. Lett. **104**, 130502 (2010).

[47] E. Prodan, T. L. Hughes, and B. A. Bernevig, Phys. Rev. Lett. **105**, 115501 (2010).

[48] A. M. Turner, Y. Zhang, and A. Vishwanath, Phys. Rev. B **82**, 241102 (2010).

[49] Z. Liu, H.-L. Guo, V. Vedral, and H. Fan, Phys. Rev. A **83**, 013620 (2011).

[50] J. Dubail and N. Read, Phys. Rev. Lett. **107**, 157001 (2011).

[51] B. A. Bernevig and N. Regnault, Phys. Rev. B **85**, 075128 (2012).

[52] B. A. Bernevig and N. Regnault, arXiv:1204.5682v1.

[53] R. B. Laughlin, Phys. Rev. Lett. **50**, 1395 (1983).

[54] J. K. Jain, Phys. Rev. Lett. **63**, 199 (1989).

[55] G. Moore and N. Read, Nucl. Phys. B **360**, 362 (1991).

[56] N. Read and E. H. Rezayi, Phys. Rev. B **59**, 8084 (1999).

[57] P. Bonderson and J. K. Slingerland, Phys. Rev. B **78**, 125323 (2008).

[58] X.-L. Qi, Phys. Rev. Lett. **107**, 126803 (2011).

[59] Y.-L. Wu, N. Regnault, and B. A. Bernevig, Phys. Rev. B **86**, 085129 (2012).

[60] T. Scaffidi and G. Möller, arXiv:1207.3539v1.

[61] Y. H. Wu, J. K. Jain, and K. Sun, arXiv:1207.4439.

[62] C. H. Lee, R. Thomale, and X. L. Qi, arXiv:1207.5587.

[63] D. Jaksch, C. Bruder, J. I. Cirac, C. W. Gardiner, and P. Zoller, Phys. Rev. Lett. **81**, 3108 (1998).

[64] S. Inouye, M. R. Andrews, J. Stenger, H. J. Miesner, D. M. Stamper-Kurn, and W. Ketterle, Nature (London) **392**, 151 (1998).

[65] M. Greiner, O. Mandel, T. Esslinger, T. W. Hänsch, and I. Bloch, Nature (London) **415**, 39 (2002).

[66] N. Syassen, D. M. Bauer, M. Lettner, T. Volz, D. Dietze, J. J. Garcia-Ripoll, J. I. Cirac, G. Rempe, and S. Durr, Science **320**, 1329 (2008).

[67] A. J. Daley, J. M. Taylor, S. Diehl, M. Baranov, and P. Zoller, Phys. Rev. Lett. **102**, 040402 (2009).

[68] A. Kol and N. Read, Phys. Rev. B **48**, 8890 (1993).

[69] D. Hofstadter, Phys. Rev. B **14**, 2239 (1976).

[70] F. D. M. Haldane and E. H. Rezayi, Phys. Rev. B **31**, 2529 (1985).

[71] N. Read and D. Green, Phys. Rev. B **61**, 10267 (2000).

[72] G. Möller and S. H. Simon, Phys. Rev. B **77**, 075319 (2008).

[73] A. Cappelli, L. S. Georgiev, and I. T. Todorov, Nucl. Phys. B **599**, 499 (2001).

[74] A. Sterdyniak, N. Regnault, and B. A. Bernevig, Phys. Rev. Lett. **106**, 100405 (2011).

[75] G. Möller and N. R. Cooper, Phys. Rev. A **82**, 063625 (2010).

[76] G. Möller and N. R. Cooper, Phys. Rev. Lett. **108**, 045306 (2012).

[77] N. R. Cooper and E. H. Rezayi, Phys. Rev. A **75**, 013627 (2007).

[78] N. R. Cooper, N. K. Wilkin, and J. M. F. Gunn, Phys. Rev. Lett. **87**, 120405 (2001).

[79] N. Regnault and T. Jolicoeur, Phys. Rev. Lett. **91**, 030402 (2003).

[80] C.-C. Chang, N. Regnault, T. Jolicoeur, and J. K. Jain, Phys. Rev. A **72**, 013611 (2005).

[81] N. Regnault and T. Jolicoeur, Phys. Rev. B **76**, 235324 (2007).